PROCEEDINGS OF SCIENCE

Creating a database of pulse waveforms for scintillator-based gamma-ray detectors

Joshua Wood[a,*] **and Dakota Davis**[b]

[a] *NASA Marshall Space Flight Center, ST12 Astrophysics Branch, Huntsville, USA*

[b] *University of Alabama-Huntsville, College of Science, 301 Sparkman Drive, Huntsville, USA*

E-mail: joshua.r.wood@nasa.gov, dd0108@uah.edu

The first Gamma-ray Burst (GRB) counterpart to a gravitational wave event, GRB 170817A, proved that monitoring for gamma-ray transients is an essential part of multimessenger astronomy. As a result, research teams, globally, are now working towards the next generation of GRB instruments. To aid this work, we are creating a database of pulse waveforms for scintillation detectors over gamma-ray energies from 30-1000 keV. This database will inform performance estimates, such as the minimum energy threshold and pulse shape discrimination ability in phoswich-style detectors. We will present initial results from the database using a Hamamatsu R12699 flat panel photomultiplier tube (PMT) coupled to NaI(Tl) and CsI(Na) scintillators.

38th International Cosmic Ray Conference (ICRC2023)
26 July - 3 August, 2023
Nagoya, Japan

ICRC2023
38th International Cosmic Ray Conference
The Astroparticle Physics Conference

*Speaker

© Copyright owned by the author(s) under the terms of the Creative Commons Attribution-NonCommercial-NoDerivatives 4.0 International License (CC BY-NC-ND 4.0).

PoS(ICRC2023)704

1. Introduction

Wide field-of-view gamma-ray instruments currently play a critical role in locating the astrophysical host systems of multimessenger events. This was demonstrated with the prompt localization of GRB 170817A by the *Fermi* Gamma-ray Burst Monitor (*Fermi*-GBM) [1], which helped initiate successful multiwavelength observations of the electromagnetic counterpart to the first confirmed binary neutron star merger, GW 170817 [2]. As a result, next generation instruments with capabilities similar to *Fermi*-GBM are essential to the future of multimessenger astronomy.

Scintillating crystals are the primary technology used on-board satellites to create wide field-of-view instruments with all-sky coverage [3–7]. These crystals emit scintillation light at optical wavelengths when hit with high-energy photons [8]. The scintillation light is then collected by a photosensor, such as a photomultiplier tube (PMT) or a silicon photomultiplier (SiPM). The photosensor converts the optical photons into an electrical signal. The electrical signal is then recorded using an analog-to-digital converter operated by a field programmable gate array (FPGA). This can be done directly at the photosensor output because modern FPGAs are capable of performing energy and pulse shape measurements through digital pulse processing techniques [10].

One challenge when designing new scintillation instruments is understanding how different crystal and photosensor choices impact the final electrical signal. This is because one must consider the luminescence of the crystal material convolved with the response of a photosensor while also accounting for additional factors such as light collection and temporal response. In addition, specifications for scintillating crystals can differ depending on the manufacturer. In this proceedings, we seek to eliminate this challenge by providing initial results from a database of electrical signals produced using a set of photosensors together with scintillators from different manufacturers. This database can be used to inform design decisions on future instruments.

2. Experimental Setup

Our experimental setup is shown in Figure 1. It consists of a scintillator and photosensor combination, highlighted in yellow, placed within a dark box. The scintillator units used in this work are shown within the inlay image and noted by the light blue outline. The analog electrical signal from the photosensor is sent to a CAEN DT5725S desktop digitizer via a RG58 coaxial cable, which is marked in orange. The digitizer accepts the analog signal from the photosensor and translates it into a digital signal, consisting of a set of voltage measurements over a 20 μs long window. The measurement points are then sent to a computer, highlighted in red, using a USB connection. Each voltage measurement is separated in time by 4 ns and we refer to the overall set of measurements for each gamma-ray interaction as a pulse waveform. The waveform data are saved as a binary file, which forms the input to our pulse waveform database script written in Python.

For this initial work, we tested three "phoswich" style detection units consisting of two 50 mm diameter scintillators combined in a 0.8 mm thick aluminum housing with a 6 mm thick quartz glass window. Table 1 describes the dimensions and materials of each unit. This set of detector units was chosen because they were readily available from ongoing work on new mission designs. Their design also has the benefit of allowing us to obtain data for two scintillators at the same time. We

PoS(ICRC2023)704

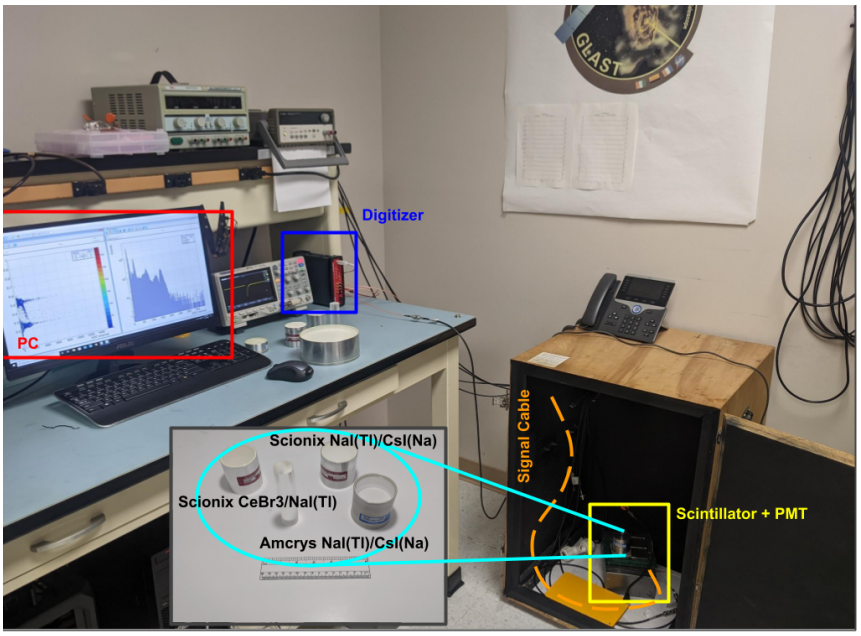

Figure 1: Experimental setup for waveform data collection.

Unit	Manufacturer	Primary Scintillator	Secondary Scintillator
1	Amcrys	15 mm NaI(Tl)	32 mm CsI(Na)
2	Scionix	15 mm NaI(Tl)	32 mm CsI(Na)
3	Scionix	11 mm CeBr	39 mm NaI(Tl)

Table 1: Thicknesses of the primary and secondary scintillator materials in each phoswich unit. Photosensors view the scintillation light created by gamma-ray interactions in each material through a 6 mm thick quartz window coupled to the back of the secondary scintillator.

then separate the waveforms for each scintillator based on the pulse shape discrimination analysis described in Section 3.

We recorded data for each phoswich unit using three sealed radioactive sources, Cs-137, Co-60 and Cd-109, placed at a distance of 75 mm from the outer diameter of the aluminum housing. This was done with two different PMTs coupled to the quartz window using BC-631 optical grease. The first photosensor was a Hamamatsu R12699 flat panel PMT operated at -900V. The second was a head-on type Hamamatsu R580 PMT operated at -1250V.

PoS(ICRC2023)704

3. Analysis

Our data analysis begins by adding the binary output file from the CAEN digitizer for each combination of scinitillator, photosensor, and gamma-ray source into a repository of raw data. We then compute a pulse shape discrimination (PSD) variable for each file in order to separate the individual waveforms according to the primary and secondary scintillator materials. It is calculated by integrating the pulse shape over two timescales, known as the long and short energy gates (Figure 2). We then formulate the PSD variable from a ratio of these two values:

$$\text{PSD} = \frac{\text{Long Gate} - \text{Short Gate}}{\text{Long Gate}} \tag{1}$$

This construction is invariant with respect to the overall waveform amplitude and only depends on the distinct decay timescale of light generated in each scintillator [11].

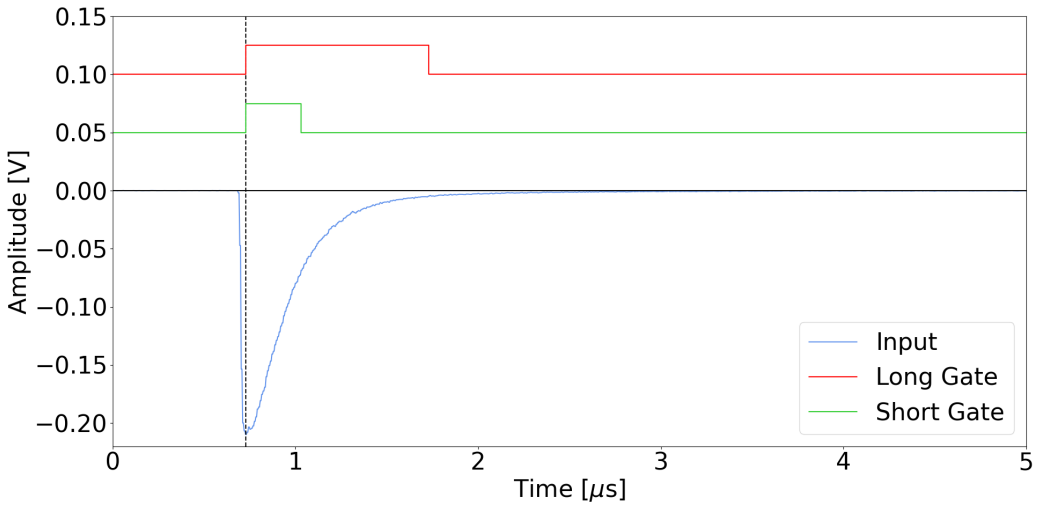

Figure 2: Long and short energy gates used to define the PSD variable in Equation 1 for a waveform generated by a NaI(Tl) scintillator.

Next, we create a two dimensional histogram of the PSD variable versus the integral of the pulse shape over the long gate (Figure 3), which acts as a proxy for the energy of gamma-ray events interacting in each scintillator. This allows us to clearly identify waveforms from the primary and secondary scintillators using the horizontal distributions that form around their characteristic PSD values. We then gather waveforms from each horizontal distribution by selecting all waveforms within a range of PSD values, referred to as a PSD cut. Histogramming the energy proxy for waveforms within this range yields the source spectrum for each scintillator, allowing us to identify the characteristic line energies present in each gamma-ray source. Finally, we apply a selection on the energy proxy near each peak, referred to as an energy cut, to select 100 waveforms at each line energy. These are stored in a separate repository of processed data.

PoS(ICRC2023)704

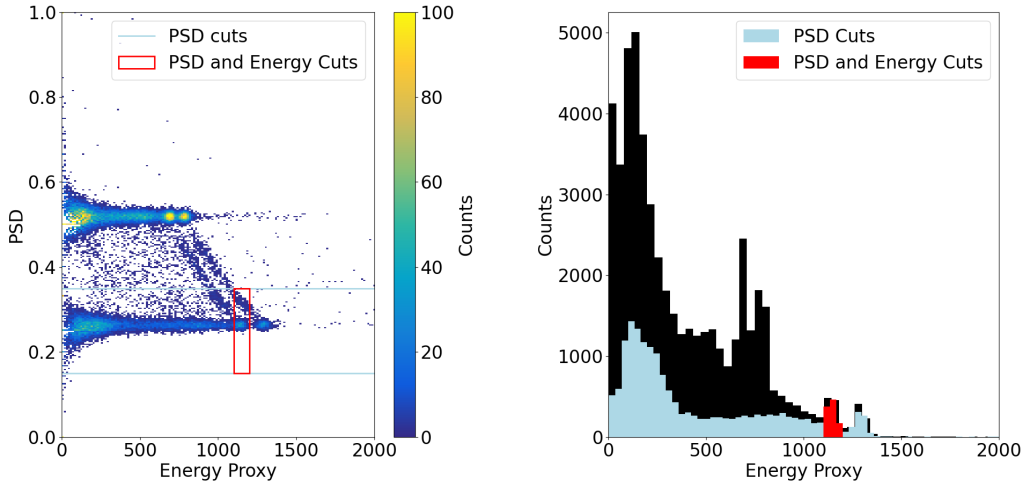

Figure 3: Histograms of PSD versus Energy Proxy and Energy Proxy for a Co-60 source. The colored overlays show the cut ranges used to select a 1173 keV gamma-ray line energy in the primary scintillator.

4. Results & Outlook

Figure 4 shows the average waveforms for gamma-ray energies of 88 keV, 662 keV, and 1332 keV recorded with the Hamamatsu R12699 flat panel PMT coupled to phoswich unit 2. These are separated according to the primary NaI(Tl) and secondary CsI(Na) scintillation materials. The peak amplitude within each material increases approximately linearly with deposited gamma-ray energy, but the overall shape differs between the two materials based on their different light output and decay timescale. In this case, the NaI(Tl) scintillator yields a larger amplitude signal because of its higher light output per keV of deposited energy as well as its faster decay time.

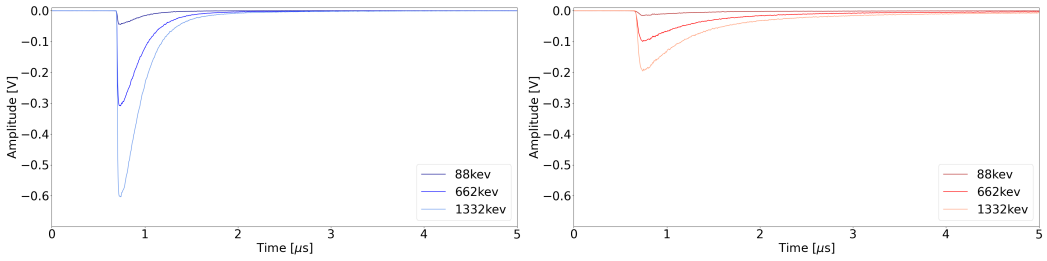

(a) **(b)**

Figure 4: Average waveforms for the 88 keV, 662 keV, and 1332 keV peaks from Cd-109, Cs-137, and Co-60 sources, respectively. These were taken with a Hamamatsu R12699 flat panel PMT coupled to phoswich unit 2 with (a) corresponding to the NaI(Tl) scintillator and (b) corresponding to the CsI(Na) scintillator.

By making these comparisons, we can estimate the minimum detectable thresholds for each scintillator. For example, only the NaI(Tl) scintillator would register events for an electronic threshold set below the level of -0.20 volts. So, in this case, the NaI(Tl) scintillator would be more desirable than the CsI(Na) scintillator. The faster decay time of NaI(Tl) also results in less waveform overlap when measuring the high photon counting rates present in the brightest GRBs, such as GRB 221009A [9]. However, there are a plethora of other considerations to take into account

PoS(ICRC2023)704

when designing new instruments, such as overall detector volume for a given mass and whether to integrate the photosensor signal before digitization. We therefore provide a data release [12] containing the waveforms from our work. These can be analyzed according to the needs of different mission designs. In the future, we plan to expand this data release with additional scintillation materials as well as different photosensors, including SiPMs.

References

[1] V. Connaughton et al., *Fermi GBM trigger 170817.529 and LIGO single IFO trigger*, GCN, 21506, 2017

[2] B.P. Abbott et al., *GW170817: Observation of Gravitational Waves from a Binary Neutron Star Inspiral*, PRL, 119, 2017

[3] G. Fishman et al., *The BATSE experiment on the Compton Gamma Ray Observatory: Status and some early results*, The Compton Observatory Science Workshop, 1992

[4] C. Meegan et al., *THE FERMI GAMMA-RAY BURST MONITOR*, ApJ, 702, 2009

[5] E. Grove et al., *Glowbug, a Low-Cost, High-Sensitivity Gamma-Ray Burst Telescope*, arxiv:2009.11959

[6] Z.H. An et al., *The design and performance of GRD onboard the GECAM satellite*, Radiation Detection Technology and Methods, 6, 2022

[7] J. Smith et al., *BurstCube: Mission Concept, Performance, and Status*, 36th ICRC, 2019

[8] G. Knoll, *Radiation Detection and Measurement*, John Wiley & Sons, Inc., 3rd ed., 2000

[9] S. Lesage et al., *Fermi-GBM Discovery of GRB 221009A: An Extraordinarily Bright GRB from Onset to Afterglow*, ApJ, 2023 [arxiv:2303.14172]

[10] V.T. Jordanov et al., *Digital techniques for real-time pulse shaping in radiation measurements*, NIM A, 353, 1994

[11] *UM5960 - CoMPASS User Manual*, Revision 14, CAEN, 2021.

[12] J. Wood and D. Davis, *Pulse Waveform Database for Scintillator-based Detectors*, v1, Zenodo [10.5281/zenodo.8157743]

PoS(ICRC2023)704